Stem Cell Reports
Report
ISSCR
OPEN ACCESS

Revealing Tissue-Specific SARS-CoV-2 Infection and Host Responses using Human Stem Cell-Derived Lung and Cerebral Organoids

Shashi Kant Tiwari,[1] Shaobo Wang,[1] Davey Smith,[2] Aaron F. Carlin,[2] and Tariq M. Rana[1,3,*]
[1]Division of Genetics, Department of Pediatrics, Program in Immunology, Institute for Genomic Medicine, University of California San Diego, 9500 Gilman Drive MC 0762, La Jolla, CA 92093, USA
[2]Division of Infectious Diseases and Global Public Health, Department of Medicine, University of California San Diego, 9500 Gilman Drive MC 0762, La Jolla, CA 92093, USA
[3]Lead contact
*Correspondence: trana@ucsd.edu
https://doi.org/10.1016/j.stemcr.2021.02.005

SUMMARY

COVID-19 is a transmissible respiratory disease caused by a novel coronavirus, SARS-CoV-2, and has become a global health emergency. There is an urgent need for robust and practical *in vitro* model systems to investigate viral pathogenesis. Here, we generated human induced pluripotent stem cell (iPSC)-derived lung organoids (LORGs), cerebral organoids (CORGs), neural progenitor cells (NPCs), neurons, and astrocytes. LORGs containing epithelial cells, alveolar types 1 and 2, highly express ACE2 and TMPRSS2 and are permissive to SARS-CoV-2 infection. SARS-CoV-2 infection induces interferons, cytokines, and chemokines and activates critical inflammasome pathway genes. Spike protein inhibitor, EK1 peptide, and TMPRSS2 inhibitors (camostat/nafamostat) block viral entry in LORGs. Conversely, CORGs, NPCs, astrocytes, and neurons express low levels of ACE2 and TMPRSS2 and correspondingly are not highly permissive to SARS-CoV-2 infection. Infection in neuronal cells activates TLR3/7, OAS2, complement system, and apoptotic genes. These findings will aid in understanding COVID-19 pathogenesis and facilitate drug discovery.

INTRODUCTION

Coronavirus disease 2019 (COVID-19), a transmissible respiratory disease caused by a novel severe acute respiratory syndrome coronavirus, SARS-CoV-2, has become a global health emergency since its outbreak in 2019 (Lu et al., 2020). There are currently no approved drugs for this disease, and there is an urgent need for developing therapeutic strategies. In addition, there is a lack of robust and practical *in vitro* model systems to investigate the pathophysiology of COVID-19. The etiologic agent of COVID-19, SARS-CoV-2, is an enveloped positive-sense single-stranded RNA virus. SARS-CoV-2 uses angiotensin-converting enzyme 2 (ACE2) as a host cell receptor and transmembrane serine protease 2 (TMPRSS2) to cleave its spike protein for entry into the host cell (Hoffmann et al., 2020). Symptoms of COVID-19 vary in severity and manifest in many ways involving multiple human organ systems. Due to the permissiveness of viral infection in various tissues, SARS-CoV-2 could lead to multiorgan failure and death (Puelles et al., 2020). Our current understanding of COVID-19 disease is based on clinical outcomes and studies using cancer cell lines or transgenic mouse models expressing ACE2 receptor for viral entry, which have limitations in recapitulating the human physiology to decipher fundamental molecular mechanisms regulating host-pathogen interactions, viral replication kinetics, and tropism. Thus, there is an urgent need for robust and practical *in vitro* model systems to investigate the pathophysiology of SARS-CoV-2 infection.

Induced pluripotent stem cells (iPSCs) or multipotent adult tissue stem cells can be differentiated to generate three-dimensional (3D) complex organoid structures containing multiple cell types and assemblies that have characteristics of spatial organization and function of a tissue (Benito-Kwiecinski and Lancaster, 2019). Organoids have shown great promise in modeling human diseases, investigating host-pathogen interactions, and drug screening. In earlier studies, we and others have utilized embryonic stem cell/iPSC-derived human neural progenitor cells (NPCs) and cerebral organoids (CORGs) to understand Zika virus-associated neuronal injury (Dang et al., 2016; Dutta and Clevers, 2017; Muffat et al., 2018; Xu et al., 2016). Recently, we reported glial cell diversity and methamphetamine-induced neuroinflammation in human CORGs by using single-cell RNA sequencing (Dang et al., 2020). Several studies using stem cell-derived organoids have started to provide further insights into SARS-CoV-2 infection of various cell types and host responses, and the discovery of new drug candidates (Han et al., 2020; Jacob et al., 2020; Katsura et al., 2020; Lamers et al., 2020; Mykytyn et al., 2021; Pellegrini et al., 2020; Ramani et al., 2020; Yang et al., 2020). Interestingly, SARS-CoV-2 productively infects brain choroid plexus epithelium, leading to cell death and functional deficits (Jacob et al., 2020; Pellegrini et al., 2020).

To investigate the tissue-specific SARS-CoV-2 infection and host responses in lungs and brain, we generated 3D human LORGs and CORGs, and brain cell types such as NPCs, neurons, and astrocytes. By using a SARS-CoV-2

This is an open access article under the CC BY-NC-ND license (http://creativecommons.org/licenses/by-nc-nd/4.0/).

pseudovirus and USA-WA1/2020 SARS-CoV-2, we determined viral tropism, host responses, and viral inhibition by specific TMPRSS2 drugs and a spike-protein-binding peptide EK1.

RESULTS

To develop a model system for investigating the human lung pathophysiology of SARS-CoV-2 infection, we differentiated stepwise human iPSCs into lung organoids (LORGs) as described previously, with minor modification (Leibel et al., 2019; Miller et al., 2019). First, we differentiated human iPSCs into definitive endoderm (DE) followed by specification into anterior foregut endoderm/spheroids (AFE), lung progenitor cells), and finally LORGs (Figures 1A, S1A, and S1B). During differentiation, we characterized the authenticity of each step of differentiation into specific cell types. AFE in LORG medium by day 12 generated an epithelial-like structure and as the organoids progressively grow, mesenchymal populations became visible, surrounding epithelial structures (Figures 1A and S1B). Next, AFE differentiation was confirmed by immunolabeling of AFE markers such as NK2 homeobox 1 (NKX2.1$^+$) cells and western blotting of NKX2.1 to confirm their differentiation into AFE cells (Figures S1C and S1D). In addition, AFE also contains progenitor cells such as SOX2$^+$ cells (Figure S1D). By day 60 (60D) in culture, human LORGs have prominent epithelial structure as visualized by hematoxylin and eosin (H&E) staining (Figure 1B). During the development of 3D LORG, we detected expression of both proximal and distal regions of lung by SOX2 and SOX9, respectively (Figure S1D). These proximal and distal regions of lung contain epithelial cells specializing in diverse functions such as secretory, basal, and ciliated cells in the airways, and type 1 and 2 cells lining the alveoli (Barkauskas et al., 2017). SOX9-expressing progenitors play a role in development of the entire lung epithelium and are involved in formation of airway and alveolar cell types in lungs (Ostrin et al., 2018). LORG epithelial cells (ECAD$^+$) were surrounded by mesenchymal cells as shown by vimentin (VIM) (Figure 1C). LORGs also showed mesenchymal cells on immunolabeling with smooth muscle markers smooth muscle actin and acetylated tubulin (Figure 1C). Furthermore, LORGs exhibited pseudostratified epithelial structures with P63$^+$ basal-like cells, lining the basal surfaces and population of ciliated cells such as FOXJ1$^+$ cells (Figure 1D). Importantly, alveolar cell markers SFTPB and SFTPC showed co-labeling with SARS-CoV-2 receptor ACE2 and protease TMPRSS2 (Figures 1E, 1F, and S1G). In addition, LORGs exhibited expression of alveolar type 1 markers AGER and HOPX (Figures S1E and S1F). Furthermore, quantitative gene expression analysis of 60D differentiated LORGs showed the presence of diverse cell types including progenitor cells markers (*SOX2* and *NKX2.1*), proximal lung epithelial cell genes (*SOX9*, *FOXJ1*, *FOXA1*, *FOXA2*, *SCB1A1*, *MUC5B*, *KRT5*, *KRT8*, *ASCL3*, and *TP63*), lung epithelial cell markers (*EPCAM*, *ECAD*, and *SPDEF*), alveolar type 1 cells (*AGER* and *HOPX*), and alveolar type 2 cells (*SFTPB*, *SFTPC*, *ABCA3*, and *SLC34A2*) as compared with iPSCs (Figures 1G–1J). Altogether, these results show that we have obtained bona fide iPSC-derived LORGs containing multiple cell types including alveolar types 1 and 2.

Since SARS-CoV-2 uses ACE2 receptor and the TMPRSS2 to cleave its S protein for entry into the cell, we quantified *ACE2* and *TMPRSS2* mRNA expression in iPSCs and LORGs. In addition, Hoffmann et al. (2020) showed that furin protease cleavage of spike protein at the S1/S2 site was essential for spike protein-mediated cell-cell fusion and entry into human lung cells. We also included analysis of expression of dipeptidylpeptidase 4 (*DPP4*), a functional receptor for MERS-CoV. We analyzed the expression of host proteases and found a significant increase in expression of all these genes in LORGs as compared with iPSCs, with increase in *ACE2/PLASMIN* being the highest, >10 fold (Figures 1K and S1H). To confirm cell-specific expression of *ACE2* and *TMPRSS2*, we performed immunostaining of LORGs, whereby our results showed that alveolar type 2 cells (SP-B and SP-C) expressed ACE2 and TMPRSS2 (Figures 1E, 1F, and S1G). Furthermore, western blot analysis of 60D organoids showed strong protein expression of ACE2 and TMPRSS2 in alveolar type 2 cells (Figure 1L). Overall, these results demonstrate that LORGs express SARS-CoV-2 receptor and co-factors required for viral entry.

To determine whether LORGs were permissive to SARS-CoV-2 infection, we constructed SARS-CoV-2 pseudovirus (GFP or luciferase) based on VSV to investigate the viral entry process (Wang et al., 2020). We inoculated LORGs with SARS-CoV-2 pseudovirus (multiplicity of infection [MOI] = 2) and analyzed for viral entry and infection at 24 h post infection based on EGFP signals (Figure 2A). Bright-field imaging of the whole LORG merged with robust EGFP signals as well as sections of LORG showed integration of EGFP, indicating successful incorporation of SARS-CoV-2 into organoids (Figure 2A). Furthermore, SARS-CoV-2 showed co-labeling with ACE2 and TMPRSS2, indicating virus binding with the receptor and internalization in the cell by TMPRSS2 proteases in LORG (Figure 2B). To quantify virus infection, we infected LORGs with SARS-CoV-2 pseudovirus expressing luciferase at MOI = 2 for 24 h. We observed a robust infection of organoids as quantified by luciferase activity (Figure 2C).

To define the S-mediated and TMPRSS2-dependent SARS-CoV-2 infection of LORGs and to assess the utility of LORGs to test drugs that could inhibit viral infection, we treated LORGs with a fusion inhibition peptide, EK1,

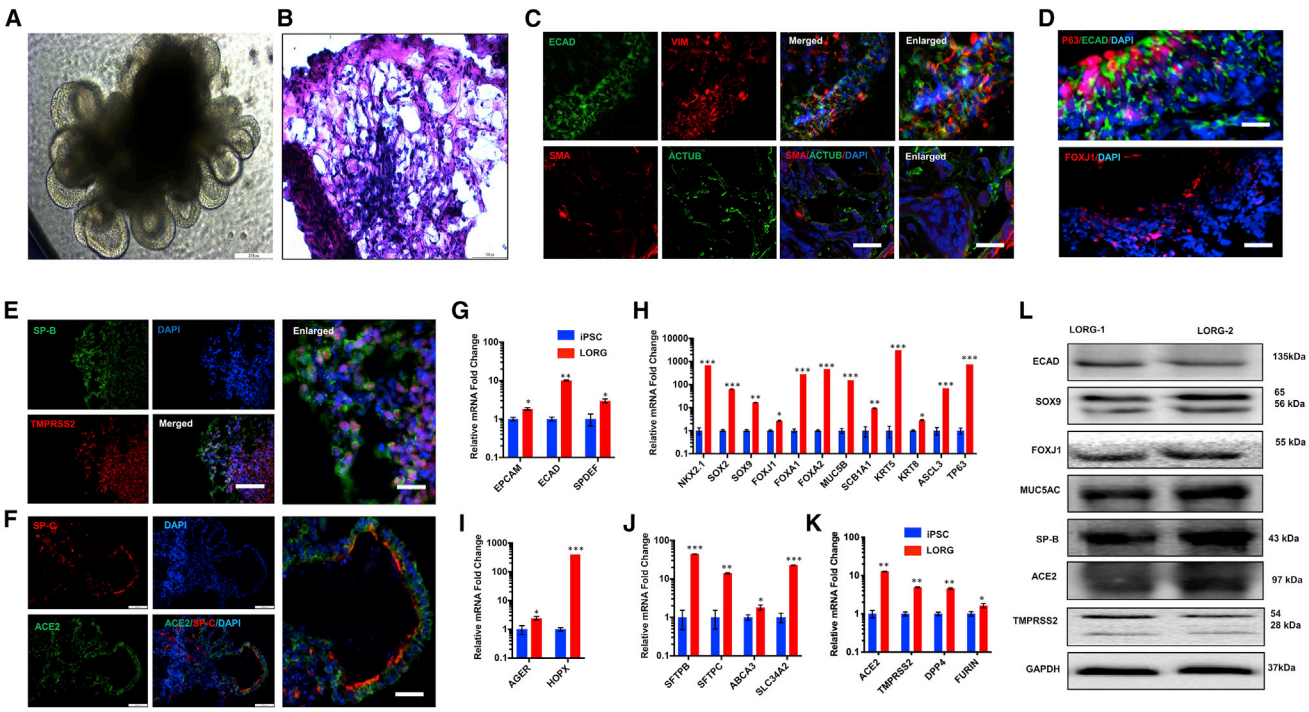

Figure 1. Human iPSC differentiation into 3D lung organoids for modeling SARS-CoV-2 infection

(A) Representative phase-contrast image of lung organoids (LORGs) at 60 days (60D). Scale bar, 200 μm.

(B) H&E staining of 60D LORG showing alveolar-like morphology. Scale bars, 100 μm.

(C) Confocal images showing labeling for cells surrounding epithelial structures (ECAD, green) co-labeled with mesenchymal-cell-type marker vimentin (VIM, red). LORGs also show mesenchymal cells by immunolabeling with smooth muscle marker, smooth muscle actin (SMA, red), and acetylated tubulin (ACTUB, green). Scale bars, 100 μm; for enlarged images, 50 μm.

(D) Epithelial structures (ECAD, green) showing basal-like cells (P63, red) on basolateral surface and ciliated cells (FOXJ1, red) on the luminal side of the epithelium. Scale bars, 100 μm.

(E and F) Representative confocal images showing labeling for alveolar type 2 cells (SP-B, green and SP-C, red) co-labeled with TMPRSS2 (E, red) or SARS-CoV-2 receptor ACE2 (F, green). Scale bars, 100 μm; for enlarged images, 50 μm.

(G) LORGs express lung epithelial cell markers *EPCAM*, *ECAD*, and *SPDEF*. Mean ± SEM of n = 3 organoids cultured in different wells. *p < 0.05, **p < 0.01 by Student's t test.

(H) Expression analysis of proximal lung epithelial cell markers (*SOX9*, *FOXJ1*, *FOXA1*, *FOXA2*, *SCB1A1*, *MUC5B*, *KRT5*, *KRT8*, *ASCL3*, and *TP63*) and progenitor cell genes (*NKX2.1* and *SOX2*) expressed in developing lungs. Mean ± SEM of n = 3 organoids cultured in different wells. *p < 0.05, **p < 0.01, ***p < 0.001 by Student's t test.

(I) Analysis of lung alveolar type 1 cell genes *AGER* and *HOPX*. Mean ± SEM of n = 3 organoids cultured in different wells. *p < 0.05, ***p < 0.001.

(J) Expression analysis of expression of lung alveolar type 2 cell genes *SFTPB*, *SFTPC*, *ABCA3*, and *SLC34A2*. Mean ± SEM of n = 3 organoids cultured in different wells. *p < 0.05, **p < 0.01, ***p < 0.001.

(K) qRT-PCR analysis of 60D LORG shows expression of *ACE2*, *TMPRSS2*, *DPP4*, and *Furin*. Data presented as mean ± SEM of n = 3 organoids cultured in different wells. *p < 0.05, **p < 0.01.

(L) Western blot analysis of 60D organoid showing protein levels for ECAD, SOX9, FOXJ1, MUC5AC, and alveolar type 2 cells (surfactant protein B [SP-B]), SARS-CoV-2 receptor (ACE2), and protease (TMPRSS2). n = 2 organoids.

See also Figure S1 and Table S1.

targeting the HR1 domain of the spike protein and TMPRSS2 inhibitor camostat, then quantified the luciferase activity. We showed that camostat or EK1 peptide inhibited viral infection, confirming that pseudovirus entry is mediated by the spike protein and is dependent on TMPRSS2 function (Figure 2C). As expected, combination of camostat and EK1 peptide robustly inhibited viral infection in LORGs (Figure 2C). Next, we compared these results with a lung epithelial cell line, Calu-3, and obtained similar results whereby EK1 peptide or TMPRSS2 inhibitors, camostat and nafamostat, repressed viral infection, which was further reduced when both classes of inhibitors were

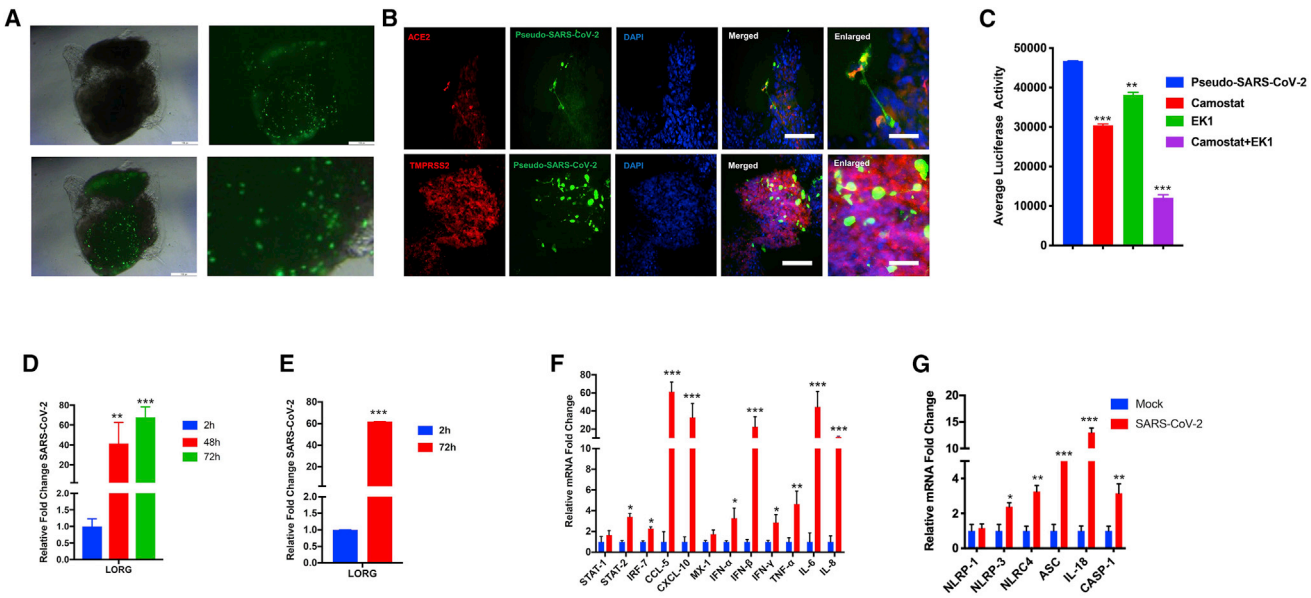

Figure 2. SARS-CoV-2 robustly replicates in human LORGs and induces expression of genes involved in innate immunity and inflammation

(A) Phase-contrast and fluorescence imaging shows infection of SARS-CoV-2-GFP pseudovirus at 24 h post infection and MOI = 2. Scale bars, 200 μm.

(B) Fluorescence image showing that SARS-CoV-2 GFP pseudovirus infects ACE2 and TMPRSS2^{+} cells of the LORG. Scale bars, 100 μm; for enlarged images, 50 μm.

(C) Pseudo-SARS-CoV-2-luciferase pseudovirus infection is blocked by viral entry inhibitors. Bar graph shows the luciferase activity in the presence and absence of TMPRSS2 inhibitor (camostat mesylate) and a fusion inhibitor EK1 peptide to LORG infected with SARS-CoV-2 pseudovirus. Mean ± SEM of n = 3 organoids cultured in different wells. ***p < 0.001 by Student's t test.

(D and E) Lung organoids were infected with SARS-CoV-2 USA-WA1/2020 virus at MOI = 2, and viral RNAs from supernatant (D) and cellular (E) fractions were quantified at indicated times of infection. Mean ± SEM of n = 2 organoids cultured and infected in different wells. **p < 0.01, ***p < 0.001 by Student's t test.

(F and G) LORGs were infected as above in (E), and gene expression of indicated genes was quantified by qRT-PCR at 72 h post infection. Bar graph shows expression of immune response genes and cytokines (F) and inflammasome markers (G). Mean ± SEM of n = 2 organoids cultured and infected in different wells. *p < 0.05, **p < 0.01, ***p < 0.001 by Student's t test.

See also Figure S1 and Table S1.

combined (Figure S1I). We then tested the inhibitory activities of nafamostat in Calu-3 cells infected with a patient-derived isolate of SARS-CoV-2, whereby our results showed that nafamostat significantly reduced SARS-CoV-2 infection (Figures S1J–S1K) as observed in LORGs. Together, these results show that iPSC-derived LORGs provide a 3D lung model system to evaluate spike protein-mediated viral infection and drug efficacy to inhibit SARS-CoV-2.

To determine the utility of the LORG model system for understanding the pathogenesis of SARS-CoV-2 infection, we used a patient-derived isolate, SARS-CoV-2 USA-WA1/2020, for LORG infection. LORGs were infected with SARS-CoV-2 USA-WA1/2020, and infection rates were quantified by evaluating viral RNA of the infected cells and supernatants. We found that the viral strain productively infected LORGs and the infection rate was increased in a time-dependent manner (Figures 2D and 2E). To investigate physiological effects of virus infection, we examined the host response genes and we found that expression of a number of immune-regulatory genes including *STAT1*, *STAT2*, interferons (*IFNs*), and chemokines were upregulated in LORGs (Figure 2F). Our results showed that *CCL5*, *CXCL10*, *IFN-β*, interleukin-6 (*IL-6*), and *IL-8* were all upregulated >10-fold, and these findings are consistent with the data obtained from SARS-CoV-2 infection of lung epithelial cells (Blanco-Melo et al., 2020) and COVID-19 patients relative to healthy donors (Daamen et al., 2020). Interestingly, our results also indicate that SARS-CoV-2 infection activates the inflammasome pathway because the key genes of this pathway including *NLRP3*, *ASC*, *IL-18*, and caspase-1 were upregulated (Figure 2G). Together, our results demonstrate that SARS-CoV-2 robustly replicates in human LORGs and provide a model system to study the mechanisms of viral pathogenesis as well as to test new therapeutics.

Clinical case reports describe a wide range of neurological and neuropsychiatric manifestations in severe COVID-19 (Helms et al., 2020). However, many questions about COVID-19 and neurological manifestations remain. (1) Does SARS-CoV-2 infect brain? (2) Which cell types in brain are infected and support viral replication? (3) What are the host responses to infection and how does the virus cause neuronal injury and observed phenotypes? To address these questions in a human-relevant *in vitro* model, we generated 3D CORGs and investigated SARS-CoV-2 infection, which was based on the brain organoid we used to investigate Zika virus infection and methamphetamine-associated neurotoxicity (Dang et al., 2016, 2020). To understand the neurotrophic potential of the SARS-CoV-2 virus, we differentiated human iPSCs into CORG, which showed presence of various cell types, such as NPCs, neurons, and glial cells characterized by their respective markers SOX-2, MAP-2, and GFAP (Figures 3A and S2A–S2D). In addition, we differentiated iPSCs into NPCs, neurons, and astrocytes, as confirmed by their characteristic markers (Figures S2B–S2D). We also quantified the mRNA expression of neural progenitor genes (*Nestin* and *SOX2*, Figure S2B), neuronal gene (*MAP2*, Figure S2C), and glial genes (*S100β* and *GFAP*, Figure S2D) in 3D CORG and in 2D NPCs, neurons, and astrocytes.

Next, to determine the potential of organoids and various cell types in brain to support SARS-CoV-2 infection, we determined ACE2 and TMPRSS2 expression in 3D CORGs as well as in differentiated NPCs, neurons, and astrocytes. qRT-PCR results showed that *ACE2* and *TMPRSS2* are expressed in CORGs and in all three cell types analyzed including NPCs, neurons, and astrocytes (Figures 3B and 3C). In addition, we analyzed the expression of host factors involved in entry and infection of SARS-CoV-2 such as *FURIN*, *PLASMIN*, *CTSL1*, *NRP1*, and *DPP4* and found upregulation of these genes in CORGs and astrocytes compared with NPCs (Figure S2E). We performed immunostaining to examine the expression of ACE2 and TMPRSS2 in organoids. ACE2/TMPRSS2 expression was readily detected with neuronal marker MAP2 (Figure 3D) and very low TMPRSS2 expression with glial cells GFAP (Figures S2F–S2I). These results show that CORGs and three cell types analyzed express *ACE2* and *TMPRSS2*, and, interestingly, *ACE2* and *TMPRSS2* expression levels were the highest in CORGs followed by neurons and astrocytes.

To determine whether CORGs were permissive to SARS-CoV-2 infection, we used SARS-CoV-2 pseudovirus (GFP or luciferase) as described above for LORGs. We inoculated CORGs with SARS-CoV-2 pseudovirus (MOI = 2) and at 24 h post infection and analyzed them for viral entry and infection based on EGFP signals (Figure 3E). Bright-field imaging of the whole CORG merged with robust EGFP signals as well as sections of CORG, indicating successful infection of SARS-CoV-2 (Figure 3E). Next, to examine the cell-specific SARS-CoV-2 pseudovirus infection, we infected neurons and NPCs with virus and carried out GFP analysis. Our results showed that infection was more efficient in neurons than in NPCs (Figures 3F and 3G), an observation that correlates with the levels of ACE2 and TMPRSS2 expression in neurons and NPCs (Figures 3B and 3C). So far, our results indicate that both LORGs and CORGs can be infected with SARS-CoV-2 GFP pseudovirus. Since major clinical complications in COVID-19 patients are lung related, we wondered about the efficiency of viral infection in LORGs and CORGs. To address this question, we infected both CORGs and LORGs with SARS-CoV-2-luciferase pseudovirus at MOI = 2, and luciferase activities were measured after 24 h of infection. Our quantification showed that viral infection was ~6-fold higher in LORGs in comparison with CORGs (Figure 3H).

To determine the cell-type-specific infectious capabilities of SAR-CoV-2 and to probe specific gene expression leading to observed clinical manifestations in COVID-19 patients, we used a patient-derived isolate, SARS-CoV-2 USA-WA1/2020, and infected NPCs, neurons, and astrocytes. All three cell types were infected under identical conditions, MOI = 2 for 48 h, and viral replication was quantified by qRT-PCR in both supernatant and cellular fractions (Figures 3I and 3J). Consistent with the pseudovirus infection results (Figures 3F and 3G), we found that the virus infected neurons more efficiently than NPCs and astrocytes. In addition, we evaluated whether these three cell types support replication of SARS-CoV-2 virus by comparing the viral RNA collected from cells at 2 h post infection. Our results indicate that all three cell types supported viral replication over time, with the amount of viral RNA being highest in neurons when compared with NPCs and astrocytes (Figures 3I and 3J).

Since virus replication levels were the highest in neurons, we analyzed host responses to viral infection in neurons. We selected genes specific to pathways that could potentially be involved in observed neurological complications in COVID-19 patients. Gene expressions from neurons infected with USA-WA1/2020 for 48 h were analyzed by qRT-PCR. Our analyses showed that SARS-COV-2 infection upregulated genes involved in innate immunity including *IL6*, *IFIT3*, *OAS2*, *TLR3*, and *TLR7*, complement system, calpain pathways, *CDK5*, apoptosis, and *RIPK1/3*-regulated necroptosis pathways (Figures 3K, 3L, 3M, and S2J). Apoptotic gene caspase-3 was upregulated while the antiapoptotic genes, *BCL2* and *BAX*, were downregulated in infected neurons (Figure 3N). Altogether, our results demonstrate that SARS-CoV-2 infects human CORGs and regulates specific gene expressions in neurons involved in neuronal functions. We also show that iPSC-derived organoids can be employed to study tissue-specific differences

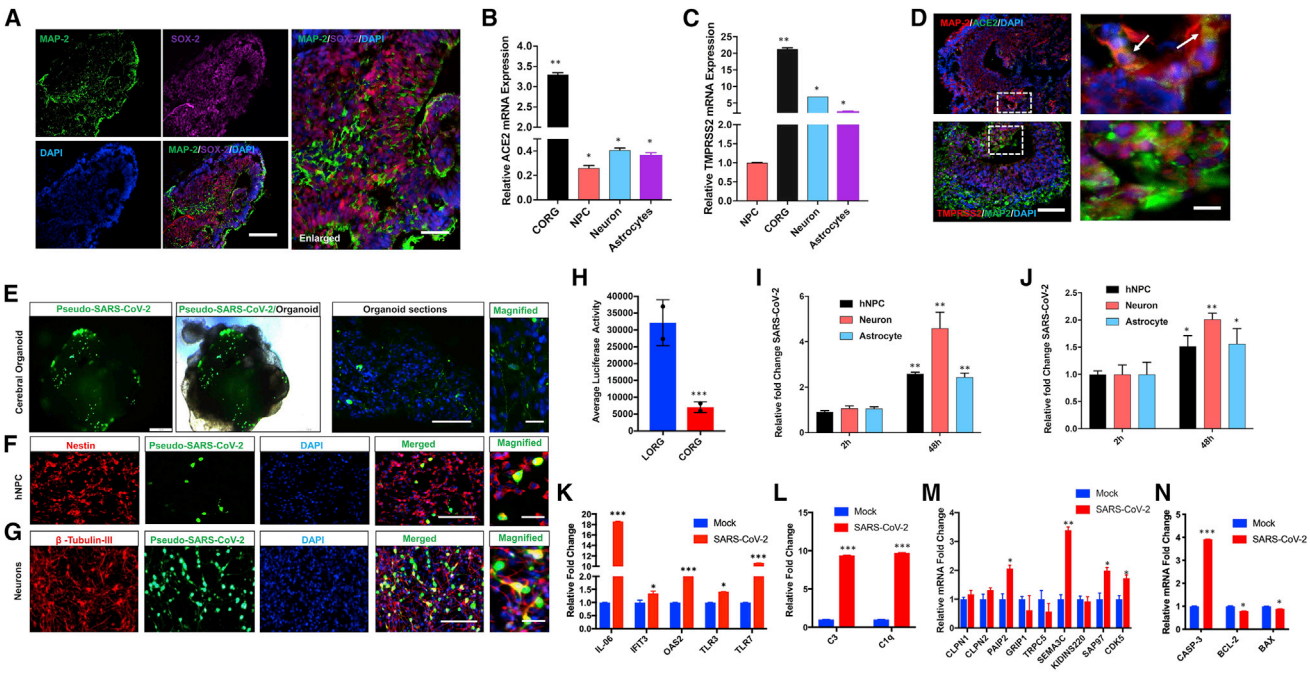

Figure 3. SARS-CoV-2 infects human cerebral organoids and activates expression of innate immunity and neurodegeneration genes in neurons

(A) Representative immunofluorescence image of an 80-day-old organoid shows various cell types including neurons (MAP-2, green), neuronal progenitor (SOX-2, magenta), and nuclear stain (DAPI, blue); merged images are also shown. Scale bars, 100 μm.

(B and C) qRT-PCR analysis shows expression of *ACE2* (B) and *TMPRSS2* (C) in CORGs, NPCs, neurons, and astrocytes. Mean ± SEM of n = 3 independent organoids and n = 3 independent experiments from NPCs, neurons, and astrocytes. *p < 0.05, **p < 0.01 by Student's t test.

(D) Confocal imaging of CORGs showing immunostaining of neuronal marker (MAP-2, red) co-labeled with SARS-CoV-2 receptor (ACE2, green) or TMPRSS2 (red) co-labeled with MAP-2 (green). White boxes were enlarged (right), and arrows show co-labeling of MAP-2/ACE2 and MAP-2/TMPRSS2 in magnified images. Scale bars, 100 μm; for enlarged images, 25 μm.

(E–G) Organoids, NPCs, and neurons were infected with pseudo-SARS-CoV-2-GFP virus at MOI = 2 and analyzed after 24 h of infection. (E) Immunofluorescence and phase-contrast images of an organoid showing SARS-CoV-2 (green). Scale bars, 200 μm. (F) Immunofluorescence confocal images of NPCs stained with antibody against Nestin (red), SARS-CoV-2 (green), and nuclear stain DAPI (blue). Scale bars, 100 μm (merged) and 25 μm (magnified). (G) Immunofluorescence confocal images of NPC differentiated neurons stained with antibody against β-tubulin-III (red), SARS-CoV-2 (green), and nuclear stain DAPI (blue). Scale bars, 100 μm (merged) and 25 μm (magnified).

(H) Organoids were infected with pseudo-SARS-CoV-2-luciferase virus at MOI = 2, and luciferase activities were measured after 24 h of infection. Mean ± SEM of n = 3 independent organoids. ***p < 0.001 by Student's t test.

(I and J) NPCs, neurons, and astrocytes were infected with SARS-CoV-2 USA-WA1/2020 virus at MOI = 2, and viral RNAs from supernatant (I) and cellular (J) fractions were quantified at indicated times of infection. Mean ± SEM of n = 3 independent organoids. ***p < 0.001, **p < 0.001, *p < 0.05 by Student's t test.

(K–N) Neurons were infected as above in (I) and (J), and gene expression of indicated genes was quantified by qRT-PCR at 48 h post infection. Bar graph shows expression of innate immune response genes (K), *C3* and *C1q* complement genes (L), synaptic function of neurons (M), and apoptotic pathway genes (N). Mean ± SEM of n = 3 independent organoids. *p < 0.05, **p < 0.01, ***p < 0.001 by Student's t test.

See also Figure S2.

in supporting viral infection as well as inducing cell-specific host responses.

DISCUSSION

The SARS family of viruses, including SARS-CoV-2, targets the human respiratory system and leads to adverse effects, as observed during the COVID-19 pandemic. However, the range of human tissues permissive to SARS-CoV-2 infection is wide and includes the heart, brain, liver, and gastrointestinal system. To understand viral tropism and investigate host-pathogen biology, we utilized iPSC-derived lung and brain organoids to investigate SARS-CoV-2 infection and host responses. We found that alveolar epithelial cells highly expressed ACE2 and TMPRSS2 (Figures 1E, 1F, and

1K) and were permissive to SARS-CoV-2 infection, and supported efficient replication kinetics (Figures 2D and 2E). In addition, host factors such as neuropilin-1 (*NRP1*), cathepsin L (*CTSL1*), *plasmin*, and kallikrein-related peptidase 13 (*KLK13*) were expressed in both LORG and CORG model systems (Figures 1K, S1H, and S2E). In response to infection, most of the key genes in innate immunity, cytokine/chemokines, and inflammasome were upregulated in LORGs (Figures 2F and 2G). For example, immunity-related genes include *STAT1/2*, *IRF7*, *CCL5*, *CXCL10*, *TNFα*, *IL-6*, *IL-8*, and *IFN*, which corroborate with the patient-derived results indicating production of a cytokine storm leading to severe lung injury. In addition, we found that SARS-CoV-2 infection of LORGs activated genes involved in inflammasome pathways (*NLRP3*, *NLRC4*, *ASC*, *IL-18*, and caspase-1), suggesting that inflammasome activation causes pulmonary inflammation and cell death in lungs.

There is growing evidence of neurological complications in people with COVID-19 (Helms et al., 2020; Kremer et al., 2020; Mao et al., 2020). However, the SARS-CoV-2 permissiveness of brain and specific cell types is not well established. Our results show that CORGs express both ACE2 and TMPRSS2 and support virus infection. Corresponding to the lower expression of *ACE2* and *TMPRSS2* in CORGs, we observed lower viral infection rates in CORGs as compared with LORGs (Figures 3B, 3C, and 3H). Similarly, neurons expressed more ACE2 and TMPRSS2 than other cell types and were more permissive to viral infection than astrocytes and NPCs (Figures 3B, 3C, 3F, 3G, 3I, and 3J). Consistent with our results, two groups reported that SARS-CoV-2 does not infect neurons but efficiently infects choroid plexus epithelium, leading to cell damage and death (Jacob et al., 2020; Pellegrini et al., 2020). Interestingly, SARS-CoV-2 infection of neurons exhibited stimulation of gene expression different from LORGs because we found *TLR*s, *OAS*, and *IL-6* but no *IFN*s (Figures 3K, 3L, and S2J). Furthermore, Zika, which is also a positive strand virus akin to SARS-CoV-2, also activates *TLR3* to cause neuronal injury in NPCs (Dang et al., 2016). In addition, complement system gene expression was strongly enhanced during SARS-CoV-2 infection, suggesting a potential mechanism for COVID-19-related symptoms whereby the complement system is activated in response to injury, infection, and neurodegenerative diseases and triggers synaptic loss and neuronal cell death. Due to enhanced inflammatory response, neurons undergo apoptotic cell death as suggested by enhanced expression of caspase-3 and downregulation of antiapoptotic genes *BCL2* and *BAX*.

Finally, we showed that viral entry was spike protein-mediated and that this was blocked by a specific inhibitor of spike protein, EK1 peptide, and TMPRSS2 inhibitors camostat and nafamostat in LORGs (Figure 2C), Calu-3 cells (Figures S1I–S1K). These results are in agreement with previous studies showing the activities of EK1 peptide (Xia et al., 2020) and TMPRSS2 inhibitors (Hoffmann et al., 2020) in repressing SARS-CoV-2, further validating the utility of stem cell-derived organoids to identify new therapeutics. Altogether, the described organoid model studies could facilitate the speed of drug discovery and provide useful knowledge about the mechanism of action and potential side effects of new drugs.

EXPERIMENTAL PROCEDURES

All studies were performed in accordance with the approved IRB protocols by the University of California, San Diego. Human iPSC cells were differentiated into LORGs and CORGs by following the previously established methods (Leibel et al., 2019; Miller et al., 2019) with minor modifications. In brief, ~75%–85% confluent undifferentiated human iPSC colonies were treated with 1 mg/mL dispase solution for 5–10 min at 37°C, washing cells gently with DMEM/F12 and scraping the colonies with a cell scraper in mTeSR^{TM1} medium. Next, iPSC colonies were dissociated into smaller colonies using serological pipette, and 0.5 mL of the smaller human iPSC clumps were plated in 24-well Matrigel-coated plates. When cells reached to 50%–75% confluence, stepwise differentiation was started into DE AFE, and LORGs. CORGs were prepared as described previously (Dang et al., 2016, 2020). Twenty 80-day organoids were transferred to bioreactors (125 mL) containing a magnetic shaft and stirring speed was maintained at 50–60 rpm. A detailed description of stem cell differentiation, immunofluorescence characterization, qRT-PCR, western blotting, viral infection, and statistical analysis is provided in Supplemental experimental procedures.

SUPPLEMENTAL INFORMATION

Supplemental information can be found online at https://doi.org/10.1016/j.stemcr.2021.02.005.

AUTHOR CONTRIBUTIONS

S.K.T. designed and performed experiments, analyzed the data, and wrote the manuscript draft; S.W. designed and performed experiments; D.S. provided resources; A.C. gave advice in experimental plans and performed experiments; T.M.R. conceived the overall project and experimental design, and participated in data analyses, interpretations, and manuscript writing.

DECLARATION OF INTERESTS

T.M.R. is a founder of ViRx Pharmaceuticals and has an equity interest in the company. The terms of this arrangement have been reviewed and approved by the University of California, San Diego in accordance with its conflict of interest policies.

ACKNOWLEDGMENTS

We thank F. Furnari for the iPSC lines and members of the Rana lab for helpful discussions and advice. The following reagent was deposited by the Centers for Disease Control and Prevention and

obtained through BEI Resources, NIAID, NIH: SARS-Related Coronavirus 2, Isolate USA-WA1/2020, NR-52281. This work was supported by a Career Award for Medical Scientists from the Burroughs Wellcome Fund USA and a grant from the National Institutes of Health USA (K08 AI130381) to AFC, John and Mary Tu Foundation USA, and in part by grants from the National Institutes of Health USA (CA177322, DA039562, DA049524, and AI125103).

Received: October 16, 2020
Revised: February 7, 2021
Accepted: February 7, 2021
Published: March 9, 2021

REFERENCES

Barkauskas, C.E., Chung, M.I., Fioret, B., Gao, X., Katsura, H., and Hogan, B.L. (2017). Lung organoids: current uses and future promise. Development *144*, 986–997.

Benito-Kwiecinski, S., and Lancaster, M.A. (2019). Brain organoids: human neurodevelopment in a dish. Cold Spring Harb. Perspect. Biol. *12*, a035709.

Blanco-Melo, D., Nilsson-Payant, B.E., Liu, W.C., Uhl, S., Hoagland, D., Moller, R., Jordan, T.X., Oishi, K., Panis, M., Sachs, D., et al. (2020). Imbalanced host response to SARS-CoV-2 drives development of COVID-19. Cell *181*, 1036–1045 e1039.

Daamen, A.R., Bachali, P., Owen, K.A., Kingsmore, K.M., Hubbard, E.L., Labonte, A.C., Robl, R., Shrotri, S., Grammer, A.C., and Lipsky, P.E. (2020). Comprehensive transcriptomic analysis of COVID-19 blood, lung, and airway. bioRxiv https://doi.org/10.1101/2020.05.28.121889.

Dang, J., Tiwari, S.K., Agrawal, K., Hui, H., Qin, Y., and Rana, T.M. (2020). Glial cell diversity and methamphetamine-induced neuroinflammation in human cerebral organoids. Mol. Psychiatry https://doi.org/10.1038/s41380-020-0676-x.

Dang, J., Tiwari, S.K., Lichinchi, G., Qin, Y., Patil, V.S., Eroshkin, A.M., and Rana, T.M. (2016). Zika virus depletes neural progenitors in human cerebral organoids through activation of the innate immune receptor TLR3. Cell Stem Cell *19*, 258–265.

Dutta, D., and Clevers, H. (2017). Organoid culture systems to study host-pathogen interactions. Curr. Opin. Immunol. *48*, 15–22.

Han, Y., Duan, X., Yang, L., Nilsson-Payant, B.E., Wang, P., Duan, F., Tang, X., Yaron, T.M., Zhang, T., Uhl, S., et al. (2020). Identification of SARS-CoV-2 inhibitors using lung and colonic organoids. Nature *589*, 270–275.

Helms, J., Kremer, S., Merdji, H., Clere-Jehl, R., Schenck, M., Kummerlen, C., Collange, O., Boulay, C., Fafi-Kremer, S., Ohana, M., et al. (2020). Neurologic features in severe SARS-CoV-2 infection. N. Engl. J. Med. *382*, 2268–2270.

Hoffmann, M., Kleine-Weber, H., Schroeder, S., Kruger, N., Herrler, T., Erichsen, S., Schiergens, T.S., Herrler, G., Wu, N.H., Nitsche, A., et al. (2020). SARS-CoV-2 cell entry depends on ACE2 and TMPRSS2 and is blocked by a clinically proven protease inhibitor. Cell *181*, 271–280.e8.

Jacob, F., Pather, S.R., Huang, W.K., Zhang, F., Wong, S.Z.H., Zhou, H., Cubitt, B., Fan, W., Chen, C.Z., Xu, M., et al. (2020). Human pluripotent stem cell-derived neural cells and brain organoids reveal SARS-CoV-2 neurotropism predominates in choroid plexus epithelium. Cell Stem Cell *27*, 937–950.e9.

Katsura, H., Sontake, V., Tata, A., Kobayashi, Y., Edwards, C.E., Heaton, B.E., Konkimalla, A., Asakura, T., Mikami, Y., Fritch, E.J., et al. (2020). Human lung stem cell-based alveolospheres provide insights into SARS-CoV-2-mediated interferon responses and pneumocyte dysfunction. Cell Stem Cell *27*, 890–904.e8.

Kremer, S., Lersy, F., Anheim, M., Merdji, H., Schenck, M., Oesterle, H., Bolognini, F., Messie, J., Henri-Feugeas, M.C., Khalil, A., et al. (2020). Neurologic and neuroimaging findings in COVID-19 patients: a retrospective multicenter study. Neurology *95*, e1868–e1882.

Lamers, M.M., van der Vaart, J., Knoops, K., Riesebosch, S., Breugem, T.I., Mykytyn, A.Z., Beumer, J., Schipper, D., Bezstarosti, K., Koopman, C.D., et al. (2020). An organoid-derived bronchioalveolar model for SARS-CoV-2 infection of human alveolar-type II-like cells. EMBO J., e105912.

Leibel, S.L., Winquist, A., Tseu, I., Wang, J., Luo, D., Shojaie, S., Nathan, N., Snyder, E., and Post, M. (2019). Reversal of surfactant protein B deficiency in patient specific human induced pluripotent stem cell derived lung organoids by gene therapy. Sci. Rep. *9*, 13450.

Lu, R., Zhao, X., Li, J., Niu, P., Yang, B., Wu, H., Wang, W., Song, H., Huang, B., Zhu, N., et al. (2020). Genomic characterisation and epidemiology of 2019 novel coronavirus: implications for virus origins and receptor binding. Lancet *395*, 565–574.

Mao, L., Jin, H., Wang, M., Hu, Y., Chen, S., He, Q., Chang, J., Hong, C., Zhou, Y., Wang, D., et al. (2020). Neurologic manifestations of hospitalized patients with coronavirus disease 2019 in Wuhan, China. JAMA Neurol. *77*, 683–690.

Miller, A.J., Dye, B.R., Ferrer-Torres, D., Hill, D.R., Overeem, A.W., Shea, L.D., and Spence, J.R. (2019). Generation of lung organoids from human pluripotent stem cells in vitro. Nat. Protoc. *14*, 518–540.

Muffat, J., Li, Y., Omer, A., Durbin, A., Bosch, I., Bakiasi, G., Richards, E., Meyer, A., Gehrke, L., and Jaenisch, R. (2018). Human induced pluripotent stem cell-derived glial cells and neural progenitors display divergent responses to Zika and dengue infections. Proc. Natl. Acad. Sci. U S A *115*, 7117–7122.

Mykytyn, A.Z., Breugem, T.I., Riesebosch, S., Schipper, D., van den Doel, P.B., Rottier, R.J., Lamers, M.M., and Haagmans, B.L. (2021). SARS-CoV-2 entry into human airway organoids is serine protease-mediated and facilitated by the multibasic cleavage site. eLife *10*, e64508.

Ostrin, E.J., Little, D.R., Gerner-Mauro, K.N., Sumner, E.A., Rios-Corzo, R., Ambrosio, E., Holt, S.E., Forcioli-Conti, N., Akiyama, H., Hanash, S.M., et al. (2018). beta-Catenin maintains lung epithelial progenitors after lung specification. Development *145*, dev160788.

Pellegrini, L., Albecka, A., Mallery, D.L., Kellner, M.J., Paul, D., Carter, A.P., James, L.C., and Lancaster, M.A. (2020). SARS-CoV-2 infects the brain choroid plexus and disrupts the blood-CSF barrier in human brain organoids. Cell Stem Cell *27*, 951–961 e955.

Puelles, V.G., Lutgehetmann, M., Lindenmeyer, M.T., Sperhake, J.P., Wong, M.N., Allweiss, L., Chilla, S., Heinemann, A., Wanner, N., Liu, S., et al. (2020). Multiorgan and renal tropism of SARS-CoV-2. N. Engl. J. Med. *383*, 590–592.

Ramani, A., Muller, L., Ostermann, P.N., Gabriel, E., Abida-Islam, P., Muller-Schiffmann, A., Mariappan, A., Goureau, O., Gruell, H., Walker, A., et al. (2020). SARS-CoV-2 targets neurons of 3D human brain organoids. Embo J. *39*, e106230.

Wang, S., Li, W., Hui, H., Tiwari, S.K., Zhang, Q., Croker, B.A., Rawlings, S., Smith, D., Carlin, A.F., and Rana, T.M. (2020). Cholesterol 25-hydroxylase inhibits SARS-CoV-2 and coronaviruses by depleting membrane cholesterol. EMBO J. *39*, e106057.

Xia, S., Liu, M., Wang, C., Xu, W., Lan, Q., Feng, S., Qi, F., Bao, L., Du, L., Liu, S., et al. (2020). Inhibition of SARS-CoV-2 (previously 2019-nCoV) infection by a highly potent pan-coronavirus fusion inhibitor targeting its spike protein that harbors a high capacity to mediate membrane fusion. Cell Res. *30*, 343–355.

Xu, M., Lee, E.M., Wen, Z., Cheng, Y., Huang, W.K., Qian, X., Tcw, J., Kouznetsova, J., Ogden, S.C., Hammack, C., et al. (2016). Identification of small-molecule inhibitors of Zika virus infection and induced neural cell death via a drug repurposing screen. Nat. Med. *22*, 1101–1107.

Yang, L., Han, Y., Nilsson-Payant, B.E., Gupta, V., Wang, P., Duan, X., Tang, X., Zhu, J., Zhao, Z., Jaffre, F., et al. (2020). A human pluripotent stem cell-based platform to study SARS-CoV-2 tropism and model virus infection in human cells and organoids. Cell Stem Cell *27*, 125–136.e7.

Stem Cell Reports, Volume *16*

Supplemental Information

Revealing Tissue-Specific SARS-CoV-2 Infection and Host Responses using Human Stem Cell-Derived Lung and Cerebral Organoids

Shashi Kant Tiwari, Shaobo Wang, Davey Smith, Aaron F. Carlin, and Tariq M. Rana

Supplemental Figure 1

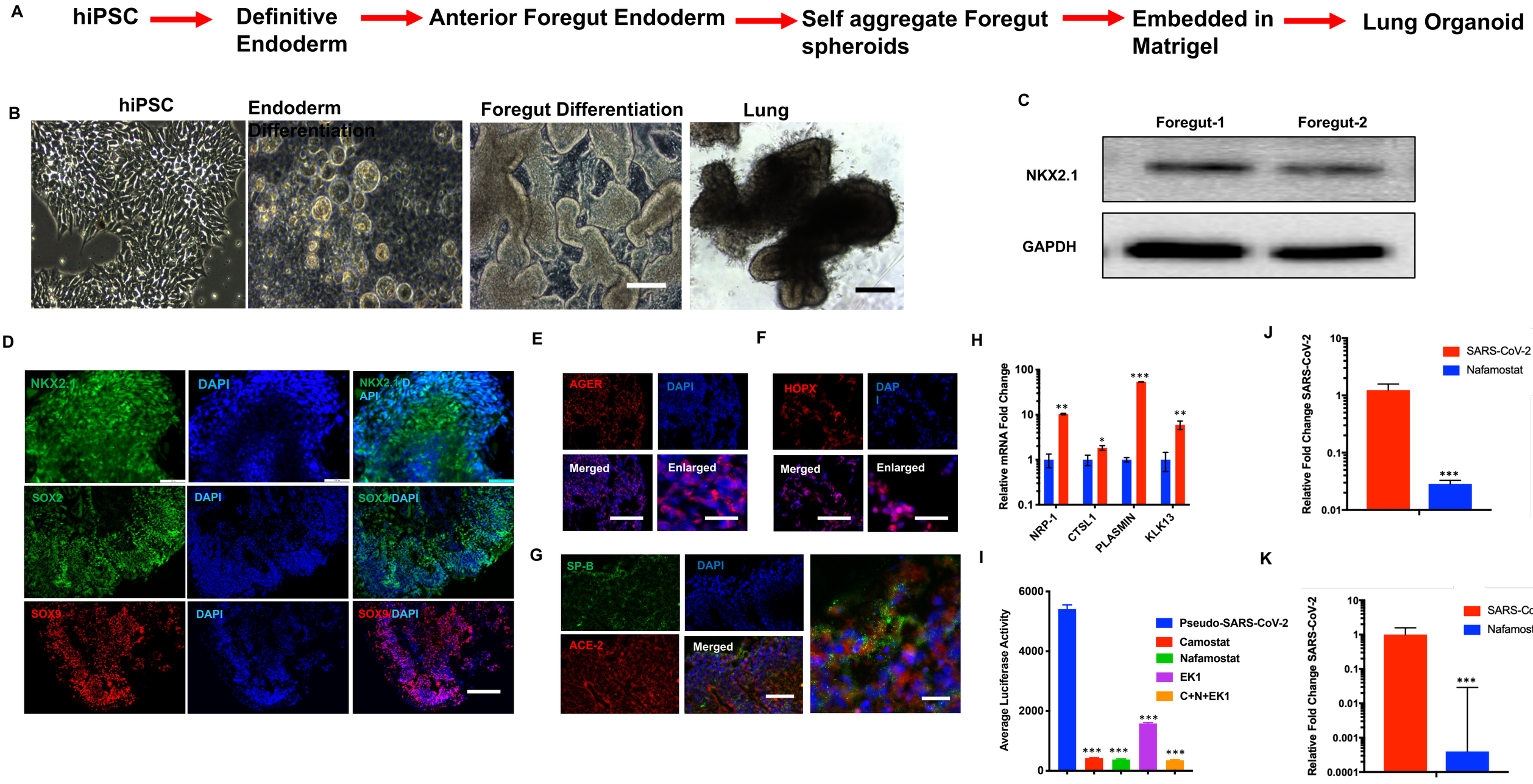

Supplemental Figure 2

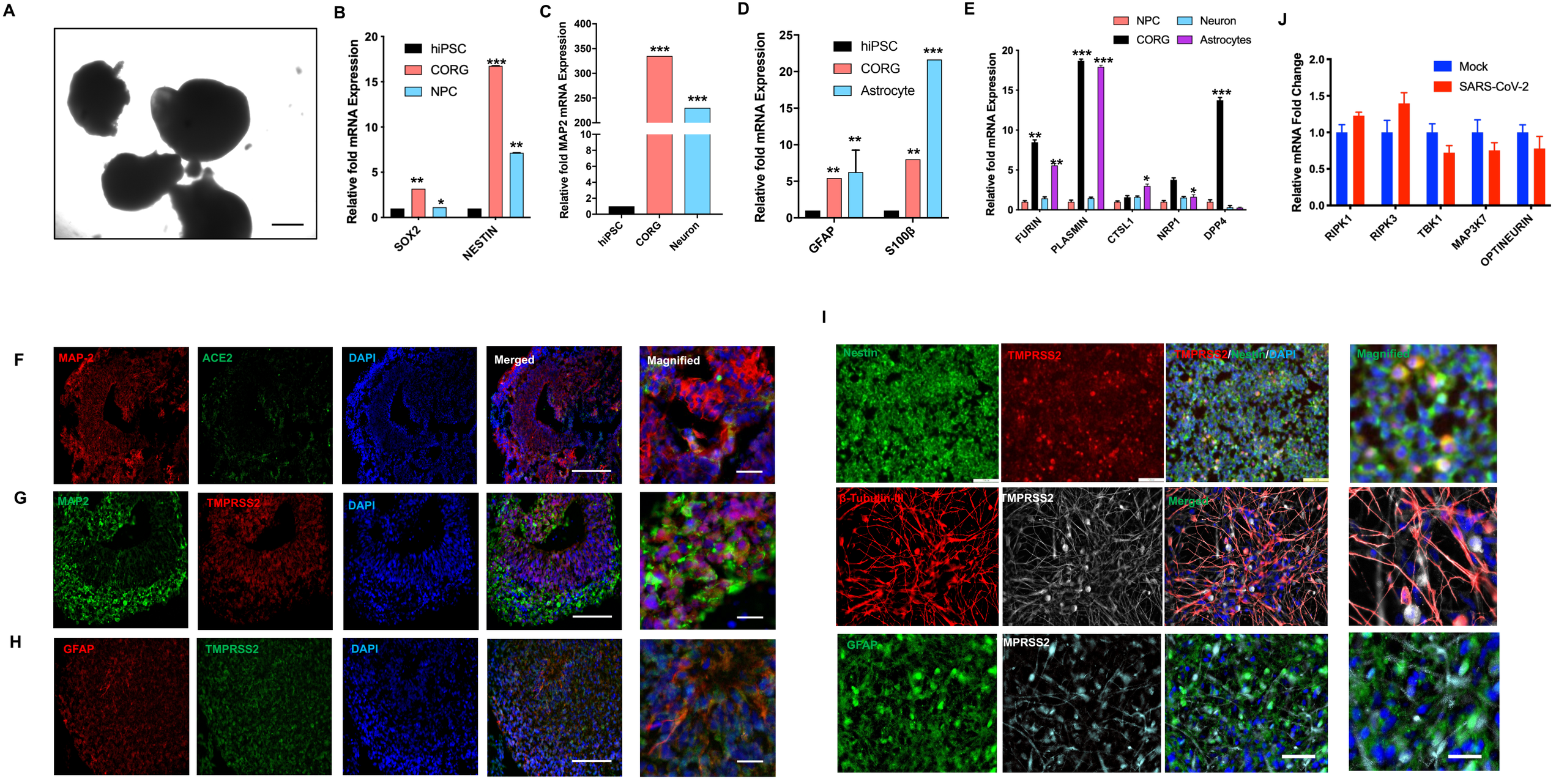

SUPPLEMENTARY FIGURE LEGENDS

Figure S1: Generation and characterization of human iPSC derived lung organoids (LORGs) for modeling SARS-CoV-2 infection.

(A) A scheme showing timeline and stepwise differentiation of human iPSC into lung organoids

(B) Brightfield phase contrast images of hiPSCs differentiation into endoderm, foregut and lung organoids. Scale bars= 100 µm

(C) Western blot for protein NKX2.1 expressed in foregut spheroids. N=2

(D) Confocal immunofluorescence images showing characteristic markers such as NKX2.1 (green), SOX2 (Red) and SOX9 (Red) in foregut spheroids and lung organoids. Scale bars= 50 µm

(E-F) Immunofluorescence images showing characteristic markers AGER and HOPX of alveolar type 1 cells in LORG. Scale bars= 200µm and for enlarged image, scale bar=50 µm

(G) Representative confocal images showing labelling of AT2 cells (SP-B, Green) co-labelled with ACE2 (Red). Scale Bars= 100µm and for enlarged image, scale bar=50µm

(H) qRT-PCR analysis shows expression of *NRP1, CTSL1, PLASMIN,* and *KLK13* in LORG. Mean ± SEM of n = 3 independent organoids, *p < 0.05, **p < 0.01 and ***p < 0.001, by Student's *t* test.

(I) Bar graph showing the luciferase activity in the presence and absence of TMPRSS2 inhibitor (Camostat and Nafamostat mesylate) and EK1 peptide to Calu 3 cells infected with pseudo-SARS-CoV-2 virus. Mean ± SEM of n = 3 independent experiments. *p < 0.05, **p < 0.01, and ***p < 0.001, by Student's *t* test.

(J, K) Inhibition of SARS-CoV-2 isolate USA-WA1/2020 infection in Calu-3 cells. Cells were infected with SARS-CoV-2 USA-WA1/2020 virus and viral RNAs from supernatant (J) and cellular (K) fractions were quantified after 48 h. Mean ± SEM of n = 3 independent experiments. ***p < 0.001, by Student's *t* test.

Figure S2: Generation and characterization of human iPSC differentiated cerebral organoid model system for SARS-CoV-2 infection.

(A) Phase contrast microscopic images of human iPSC differentiated 80 days old cerebral organoids (CORG). Scale bar represents 200 µm

(B) qRT-PCR for mRNA expression of neural stem/progenitor genes (Nestin and SOX-2) in cerebral organoid (Mean ± SEM of n = 3 independent organoids) and NPC (Mean ± SEM of n = 3 independent experiments). ***p < 0001, **p < 0.001, *p < 0.05, by Student's *t* test.

(C) qRT-PCR showing mRNA expression of neuronal gene MAP-2 in cerebral organoid (Mean ± SEM of n = 3 independent organoids) and 2D neurons. (Mean ± SEM of n = 3 independent experiments) ***p < 0001, by Student's *t* test.

(D) qRT-PCR for mRNA expression of astrocyte genes (GFAP and S100β) in cerebral organoid (Mean ± SEM of n = 3 independent organoids) and 2D astrocytes (Mean ± SEM of n = 3 independent experiments). ***p < 0001, **p < 0.001, by Student's *t* test.

(E) qRT-PCR analysis shows expression of host factors *FURIN, PLASMIN, CTSL1, NRP1* and *DPP4* in CORG. Mean ± SEM of n = 3 independent organoids and 2D NPC, neurons and astrocytes (Mean ± SEM of n = 3 independent experiments). *p < 0.05, **p < 0.01 and ***p < 0.001, by Student's *t* test.

(F) Confocal imaging of cerebral organoid immune stained with antibody against MAP-2 (Neuronal marker, red) co-labelled with antibody against ACE2 (SARS-CoV-2 receptor, green), and counterstained with nuclear stain DAPI (Blue). Magnified images show co-labelling of MAP-2/ACE2. Scale bar represents 100 μm and 25 μm.

(G) Confocal imaging of cerebral organoid immunostained with antibody against MAP-2 (Neuronal marker, Green) co-labelled with antibody against TMPRSS2 (SARS-CoV-2 effective protease, Red) counterstained with nuclear stain DAPI (Blue). Magnified images showing co-labelling of MAP-2/TMPRSS2. Scale bar represents 100 μm and 25 μm.

(H) Confocal imaging of cerebral organoid immunostained with antibody against GFAP (Astrocyte marker, red), co-labelled with antibody against TMPRSS2 (SARS-CoV-2 effective protease, green), and counterstained with nuclear stain DAPI (Blue). Magnified images show co-labelling of GFAP/TMPRSS2. Scale bar represents 100 μm and 25 μm.

(I) Immunofluorescence images showing expression of TMPRSS2 in various cell types: hNPC (Nestin, Green), Neurons (β-Tubulin-III, Red) and astrocytes (GFAP, Green). Scale bar represents 100 μm and 25 μm.

(J) qRT-PCR showing mRNA expression of genes regulating cell death and inflammation in neurons. Mean ± SEM of n = 3 independent experiments.

Table S1. List of primers

hsaACE2-Fwd	TGGGACTCTGCCATTTACTTAC
hsaACE2-Rev	CCCAACTATCTCTCGCTTCATC
hsaTMPRSS2-Fwd	GGAGTGTACGGGAATGTGATG
hsaTMPRSS2-Rev	GGACGAAGACCATGTGGATTAG
hsaNKX2-1-Fwd	GCAAAGAGGACTCGCTTGTA
hsaNKX2-1-Rev	AGTGACAAGTGGGTTATGTTGA
hsaEPCAM-Fwd	GCAGTTGTTGCTGGAATTGT
hsaEPCAM-Rev	GCATCTCACCCATCTCCTTTAT
hsaKRT8-Fwd	GCAGATCAAGACCCTCAACA
hsaKRT8-Rev	CACTTGGTCTCCAGCATCTT
hsaFOXA1-Fwd	AGGGCTGGATGGTTGTATTG
hsaFOXA1-Rev	GTGTCTGCGTAGTAGCTGTTC
hsaECAD/CDH1-Fwd	GTCATTGAGCCTGGCAATTTAG
hsaECAD/CDH1-Rev	GTTGAGACTCCTCCATTCCTTC
hsaFOXA2-Fwd	GGCCAGAGTTCCACAAATCTA
hsaFOXA2-Rev	CCCTCCCTCCTTCTTGAAATAAT
hsaSOX2-Fwd	GAGAGAAAGAAGAGGAGAGAGAAAG
hsaSOX2-Rev	GCCGCCGATGATTGTTATTATT
hsaSOX9-Fwd	TGACCTATCCAAGCGCATTAC
hsaSOX9-Rev	GCTTGCTCTGAAGAGGGTTTA
hsaTP63-Fwd	AGACAAACTGCTTCCCTTACTT
hsaTP63-Rev	GGCCCTAGTGTTACCTGAATAG
hsaKRT5-Fwd	CATGGAGATTGCCTCTTCTAGG
hsaKRT5-Rev	TCTCCTGGGAACCAAAGAATG
hsaFOXJ1-Fwd	GTTTGGGTTTGGTGGTTTGG

hsaFOXJ1-Rev	CCAGTTAAGCCTCAGCTACAG
hsaSCGB1A1-Fwd	TGGTCACACTGGCTCTCT
hsaSCGB1A1-Rev	TTCCATGGCAGCCTCATAAC
hsaMUC5B-Fwd	GAGTGGTTTGATGAGGACTACC
hsaMUC5B-Rev	CTTAGGCTGCTGGCATAAGT
hsaSPDEF-Fwd	AGCTATGGCCGCTTCATTAG
hsaSPDEF-Rev	GCTCAGCTTGTCGTAGTTCA
hsaASCL3-Fwd	AAGGAATGAGCGGGAAAGG
hsaASCL3-Rev	GCTGAGTCGCTTCTCCAAATA
hsaPDPN-Fwd	TCCCAAAGTGCTGGGATTAC
hsaPDPN-Rev	CTCATCCAGCTCTTCTCATTCC
hsaSFTPC-Fwd	CTCCACATGAGCCAGAAACA
hsaSFTPC-Rev	GAGAAGGTGGCAGTGGTAAC
hsaSFTPB-Fwd	CCGCACCCTTAAGAAGGTATTT
hsaSFTPB-Rev	CGGTGGAGTTAGGAGCAATTT
hsaABCA3-Fwd	GAGAAGGAAAGGAGGCTGAAG
hsaABCA3-Rev	GGAGGAAGAGGAAGAACAAGAG
hsaFurin-Fwd	GACGGCTACACCAACAGTATC
hsaFurin-Rev	GTCACGATCTGCTTCTCATTCT
hsaDPP4-Fwd	TGTGAGCTGAATCCGGAAAG
hsaDPP4-Rev	CACGCTGCTGTGTAGAGTATAG
hsaANPEP-Fwd	GTTCTCCTTCTCCAACCTCATC
hsaANPEP-Rev	CTGTTTCCTCGTTGTCCTTCT
hsaOAS2-Fwd	CTGGAGCTGGTCACACAATATC
hsaOAS3-Rev	GAAACTTCCTCACGGTCTCATC

hsaTLR3-Fwd	CCCTGGTGGTCCCATTTATTT
hsaTLR3-Rev	CTCAACTGGGATCTCGTCAAAG
hsaTLR7-Fwd	TTTCCCAGAGCATACAGCTTAG
hsaTLR7--Rev	GCCTCTGATGGGACAAGTAAA
hsaIFIT3-Fwd	AGTGGCTCATGCCTGTAATC
hsaIFIT3--Rev	AGACGGGATTTCACTGTGTTAG
hsaHOMER1-Fwd	GGTACACTCTGGTGTTCTCTAATC
hsaHOMER1-Rev	CTCAGCTGCCTTCGTTAGTT
has-C1q-Fwd	ACAGTAGGGCTTGGTGAATG
has-C1q-Rev	CTGGGACACAGAGTTGAATTAGA
has-C3-Fwd	CAGCAGATGACCCTGAAGATAG
has-C3-Rev	TGCGTCAGTTTGTTCTTCTTATTC
hsaCAPN1-F	CCCAATTCCTCCAAGACCTATG
hsaCAPN1-R	GGTAGCTCCATCCACAATGAA
hsaCAPN2-F	GTGACTTCCTGAGGCACTATTC
hsaCAPN2-R	CCTCCAGTTCCCATCCATTT
hsaTRPC5-F	CTGGTGGAACCTGATGGATTT
hsaTRPC5-R	CCCTTGGACGAGAACCATTATAC
hsaSEMA3A-F	GGATCAGCCGTGTGTATGTATAG
hsaSEMA3A-R	TTGATAAGGCACCCATTGATAGT
hsaCDK5-F	GACCAAGCTGCCAGACTATAAG
hsaCDK5-R	CTCCCTGTGGCATTGAGTTT
hsaGRIP1-F	GCCACAGAAACTCTCTCTTCTC
hsaGRIP1-R	CCATCACTCTGTCTCCAATCTG
hsaSAP97/DLG1-F	TGCACAATATCGACCTGAAGAA
hsaSAP97/DLG1-R	AGAGAACCTGACCCTGAACTA

hsaKIDINS220-F	AAAGCCGAAGGGAAAGTAGAG
hsaKIDINS220-R	AGGAGCGCATCCGATAAATAC
hasPAIP2-F	GAAGAGGAGTTATGGGAAGAAGAA
hasPAIP2-R	GGAGATCTCGAGCTGGAATAAA
nCoV-N1-F	GAC CCC AAA ATC AGC GAA AT
nCoV-N1-R	TCT GGT TAC TGC CAG TTG AAT CTG
hRIPK1-F	CTGGAGAGGGAACAGGAAATG
hRIPK1-R	GTACACAGAGTAAACCGAGGAAG
hRIPK3-F	GACTCCAGAGACCTCAACTTTC
hRIPK3-R	CCAGTTCATGCCTTGTCTCT
hOptineurin-F	AGGAGAAGGAAGGAAGGAGAA
hOptineurin-R	GCTCGCATCAACCAAACATAAA
hTBK1-F	GAAGGGCCTCGTAGGAATAAAG
hTBK1-R	CCCGAGAAAGACTGCAAGAA
hMAP3K7/TAK1-F	CACGCAATGAGTTGGTGTTTAC
hMAP3K7/TAK1-R	GGTTTCAGGTCCCTGTGAATTA

SUPPLEMENTAL EXPERIMENTAL PROCEDURES

Key Resources Table

Reagent	Source	Catalogue Number
Antibodies		
Mouse anti-FOXJ1	eBioscience	14-9965-82
Mouse anti-surfactant protein B (SFTPB)	Seven Hills Bioreagents	Wmab-1B9
Rabbit anti-Prosurfactant Protein C (proSP-C)	Millipore	AB3786
Rabbit anti-RAGE	Abcam	Ab216329
Mouse anti-Hop (E-1)	Santa Cruz	Sc-398703
Rabbit anti-NKX2.1	Abcam	ab76013
Rabbit anti-SOX9	Millipore	AB5535
Rabbit anti-ECAD	Cell Signaling Technology	3195
anti-CC10 (SCGB1A1)	Santa Cruz	sc-365992
Rabbit Anti-ACE2	Novus Biologicals	NBP2-67692
Rabbit anti-TMPRSS2	Abcam	Ab92323
Rabbit anti-Sox2	Abcam	ab97959
Rabbit anti-Ki67	Millipore	AB9260
GFAP (anti-mouse)	Sigma-Aldrich (USA)	G3893
Sox2 (anti-rabbit)	Abcam, (USA)	ab97959
β-Tubulin III (anti-mouse)	Abcam, (USA)	ab7751–100

Nestin (anti-chicken,)	Abcam, (USA).	ab134017
Ki67 (anti-rabbit,),	Millipore	AB9260
MAP2 (anti-chicken)	Abcam, (USA)	ab5392
Alexa Fluor 488, 594, and 647 conjugated secondary antibodies	Molecular Probes (Invitrogen, USA).	A11032, A11034, A11012, A11039, A11001
Antifade mounting medium with DAPI	Vectashield, Vector Laboratories, CA	H-1200
Chemicals		
1-thioglycerol	Sigma-Aldrich	M6145
L-ascorbic acid	Tocris Bioscience	4055
Bovine serum albumin (BSA)	Fischer Scientific (Gibco, Invitrogen, USA)	BP9703–100
Protease and phosphatase inhibitors cocktail	Pierce (USA)	A32955
Bio-Rad DC protein assay kit	Bio-Rad, USA	5000112
Chemiluminescence substrate	Thermo Scientific (USA)	34580
Optimal cutting temperature (OCT) compound	Tissue-Tech (USA)	4583
RIPA Buffer	Teknova	R3792
beta-mercaptoethanol	Sigma-Aldrich (USA)	M7522
Bio-Rad DC protein assay kit	Thermo Scientific (USA)	5000112
Chemiluminescence substrate	Thermo Scientific (USA)	34580
Immun-Blot PVDF Membrane	Bio-Rad Laboratories	1620177

Optimal cutting temperature (OCT) compound	Tissue-Tech (USA).	4583
Growth Factors		
Activin A	R&D Systems	338-AC
FGF10 (recombinant human fibroblast growth factor 10)	R&D Systems	345-FG
FGF4 (recombinant human fibroblast growth factor 4)	R&D Systems	7460-F4
FGF7 (recombinant human fibroblast growth factor 7)	R&D Systems	251-KG/CF
NOGGIN	R&D Systems	6057
Smoothened agonist (SAG)	Enzo Life Sciences	ALX-270-426-M001
Epidermal growth factor (EGF)	Sigma-Aldrich (USA)	E9644
Basic fibroblast growth factor (bFGF)	Sigma-Aldrich (USA)	F0291
Epidermal growth factor (EGF)	Sigma-Aldrich (USA)	E9644
Cell Lines		
Human induced pluripotent stem cell (hiPSC)	Cell Application	hiPS11-10
293FT	ATCC	
Calu-3	ATCC	ATCC® HTB-55™
Culture Medium		
Advanced DMEM	Thermo Fisher Scientific	12491015
CHIR-99021	Stemcell Technologies	72054

GlutaMAX (100X)	Thermo Fisher Scientific	35050061
HEPES buffer (1M)	Thermo Fisher Scientific	15630080
mTeSR^{TM1}	(Stemcell Technologies	85850
N-2 supplement	Thermo Fisher Scientific	17502048
Penicillin–streptomycin (100X)	Thermo Fisher Scientific	15140122
RPMI 1640 medium	Thermo Fisher Scientific	11875119
Matrigel basement membrane matrix growth factor reduced	Corning	354230
Matrigel basement membrane matrix	Corning	354234
DMEM-F12 medium	Thermo Fisher Scientific	11320082
MEM nonessential amino acids (MEM-NEAA)	Thermo Fisher Scientific (Gibco, Invitrogen, USA)	11140050
N2 supplement	Thermo Fisher Scientific (Gibco, Invitrogen, USA)	17502048
B-27 supplement without vitamin A	Thermo Fisher Scientific (Gibco, Invitrogen, USA)	12587010
B-27 supplement with vitamin A	Thermo Fisher Scientific (Gibco, Invitrogen, USA)	17504044
glutamine/glutaMAX, 200mM	Thermo Fisher Scientific (Gibco, Invitrogen, USA)	35050061, A2916801
Dispase	Thermo Fisher Scientific (Gibco, Invitrogen, USA)	17105–0412q
Collagenase IV	Thermo Fisher Scientific (Gibco, Invitrogen, USA)	17104019

Fetal bovine serum	Thermo Fisher Scientific (Gibco, Invitrogen, USA)	10438–018
Bovine serum albumin (BSA)	Fischer Scientific (Gibco, Invitrogen, USA).	BP9703–100

Human induced pluripotent stem cell (hiPSC) maintenance and preparation of Lung organoids

All studies were performed based on the approved IRB protocols by the University of California (UCSD), San Diego. Human induced pluripotent stem cell (hiPS11-10) from Cell Application (a kind gift from Frank Lab at UCSD) were cultured on basement membrane growth-factor-reduced Matrigel coated plate in mTeSR^{TM1} medium following previously established protocols. These iPSC cells were differentiated into the human lung organoids by following the previously established protocol by (Leibel et al., 2019; Miller et al., 2019)) with minor changes. In brief, ~75–85% confluent undifferentiated hiPSC colonies were treated with 1 mg/mL dispase solution for 5-10 min at 37^{0}C followed by removal of dispase, washing cells gently with DMEM/F12 and scraping the colonies with a cell scraper in mTeSR^{TM1} medium. Next collected iPSC colonies were dissociated into smaller colonies using serological pipette and plated 0.5mL of the smaller hiPSC clumps in 24-well Matrigel coated plate. When cells reached to 50-75% of confluency, then start stepwise differentiation into definitive endoderm, anterior foregut endoderm and lung organoid differentiation as follows:

1) Definitive Endoderm differentiation: Feed cells for 4 days with definitive endoderm differentiation medium daily by replacing existing medium. Day 1 medium consist of RPMI+100ng/mL Activin A, while Day 2 media contain RPMI+0.2% FBS+100ng/mL Activin A and Day 3 and 4 contains RPMI+2% FBS+100ng/mL Activin A.

2) Anterior foregut endoderm differentiation: At day 5 replace the medium with anterior foregut endoderm differentiation basal medium consists of Advanced DMEM/F12, 1× N-2, 1× B27, 10 mM HEPES buffer, 1× L-glutamine (2 mM), 1× penicillin–streptomycin, 0.4μM monothioglycerol, 0.25% BSA and 50 μg/mL ascorbic acid. This medium was supplemented with 10μM SB431542, 200 ng/mL Noggin, 1μM SAG, 500 ng/mL FGF4, and 2μM CHIR-99021. Change the medium every day and observe the formation of spheroid around 8 and 9 days of culture.

3) 3D Lung organoid culture: Collected foregut differentiated endoderm spheroids were mixed with Matrigel and quickly make individual droplet of 25µL on sterile parafilm and placed in incubator to solidify the Matrigel for ~10 min. To differentiate into lung organoid, each droplet were transferred into individual well of 24 well plate with basal media containing advanced DMEM/F12, 1× N-2, 1× B27, 10 mM HEPES buffer, 1× L-glutamine (2 mM), 1× penicillin–streptomycin, 0.4µM monothioglycerol, 0.25% BSA and 50 µg/mL ascorbic acid. This medium was supplemented with 3D step 1 media (FGF7 (10ng/mL, FGF10 (10ng/mL, CHIR (3µM) and EGF (10 ng/ml) added every other day for 8 days. On day 25 and onwards, the media was changed to 3D step 2 medium consisting of FGF7 (10ng/ml), FGF10 (10ng/ml), CHIR (3µM), ATRA (50nM), EGF (10ng/ml) and VEGF/PIGF (10ng/ml) and changed every 2 days for 8 days. Next step 2 media were supplemented with cAMP (100µM), IBMX (100 µM) and Dexamethasone (50nM) to continue the culture conditions. For maintenance of longer culture re-embed the organoid at every 2-3 weeks in Matrigel. We utilized 60D old lung organoids to characterize for expression of specific markers and SARS-CoV-2 infection studies.

Cerebral organoids

hiPS11-10 were cultured on basement membrane growth-factor-reduced Matrigel coated plate in mTeSR-TM[1] medium following previously established protocols. Feeder-dependent hESCs were detached from their feeder layer using 1 mg/ml collagenase (dissolved in DMEM-F12 medium) for 15–20 min at 37 °C in CO2 incubator and 0.5 mg/ml dispase (dissolved in DMEM-F12 medium) for an additional 15 min at 37°C in CO_2 incubator. Wells were washed with media to collect floating undifferentiated hESCs and colonies were dissociated using Accumax or Versene solution at 37°C for 10 min to generate a single-cell suspension. At day 0, embryoid bodies were formed using the hanging drop method with 4500 cells/drop in DMEM/F12 media supplemented with 20% knockout serum replacement (KOSR), bFGF (4 ng/ml), MEM nonessential amino acids (MEM-NEAA, 1%, vol/vol), and glutamine (200 mM, 1%, vol/vol) or grown in microwell plates. After 2 days of hanging drop culture, embryoid bodies were transferred to sterile petri dishes with refreshed media. After 6 days in culture, embryoid bodies were transferred to new petri dishes containing neural induction media consisting of DMEM/F12, N2 supplement (1%, vol/vol), MEM-NEAA (1%, vol/vol), glutamine (200 mM, 1%, vol/vol), and heparin (1µg/ml) until day 11. At day 11, organoids were transferred to Matrigel droplets (30µl) and cultured in 1:1 mixture of DMEM/F12 and Neurobasal medium supplemented with B-27 without vitamin A (1%, vol/vol), N2 (1%, vol/vol), NEAA (1%, vol/vol), insulin, beta-mercaptoethanol, and glutamine (200 mM, 1%, vol/vol). Twenty 80 days organoids were then

transferred to stir flask bioreactors (125 ml) containing magnetic shaft and stirring speed was maintained 50–60 rpm. For long term growth on day 15 in 75–100 ml of cerebral organoid differentiation media with vitamin A. Media was changed every 3 days.

Astrocyte differentiation

NPCs were plated on Matrigel coated plates in complete NPC medium at 2.5×10^4 cells/cm^2. After 2 days of NPC culture, the media was changed to astrocyte differentiation medium which consists of D-MEM supplemented with GlutaMAX-I (2 mM, 1%, vol/vol), N-2 (1%, vol/vol), FBS (1%, vol/vol), and Antibiotic-Antimycotic solution (1%, vol/vol) and then changed the media at every 3-4 days for 1 month.

Neuronal differentiation

To differentiate NPCs into the neurons, hNPCs were plated in polyornithine and laminin-coated culture dishes in complete NPC medium at $2.5–5 \times 10^4$ cells/cm^2. After 2 days, the media was changed to neural differentiation medium consisting of neurobasal medium supplemented with GlutaMAXI (200 mM, 1×, vol/vol), B-27 serum-free supplement (1×, vol/vol), and antibiotic - antimycotic (1×, vol/vol) solutions and changed medium at every 3–4 days for 2 weeks.

Cell Lines maintenance

293FT and Calu-3 cells were cultured and maintained under standard culture conditions at 37°C in a 5% CO_2 atmosphere. In brief, 293FT human embryonic kidney cells were cultured in Dulbecco's modified Eagle's medium (DMEM) supplemented with 10% FBS. Calu-3 cells are human lung airway epithelial cells, cultured in Eagle's Minimum Essential Medium (EMEM) with 10% FBS and 1% antibiotic-antimycotic solutions.

Sectioning of organoids for immunofluorescence analysis

Before sectioning, the organoids (LORG and CORG) were washed with phosphate buffer saline (PBS) to remove the residual culture medium and surrounding Matrigel was removed by incubating in cell recovery solution for 30 min. Cell recovery solution is used to recover cells or organoids from matrigel matrix for subsequent sectioning and biochemical analyses. Next after washing the organoids with PBS, fixed with 4% paraformaldehyde (PFA) for 1h followed by again washing organoid three times with PBS, stained with hematoxylin for 5 min and incubated in 30% sucrose overnight. Sucrose solution was removed, organoids were washed with PBS and embedded in OCT compound for cryosectioning. We typically cut 20-µm-thick sections of

organoid for immunohistochemical analysis using cryostat. Cryosections were blocked in 3% BSA in PBS for 1h, washed three times with PBS + 0.1% Tween-20 (PBST), and incubated at 4°C overnight with primary antibodies: ECAD (1:500, Rabbit), Sox2 (1µg/ml, Rabbit), Ki67 (1:200, Rabbit), NKX2.1 (1:500, Rabbit), Vimentin (1:200, Rabbit), SOX9 (1:200, Rabbit), FOXJ1 (1:200, Mouse), Mucin5AC (1:200, Rabbit), Surfactant protein B, SP-B (1:200, Mouse), ACE2 (1:200, Rabbit) and TMPRSS2 (1:200, Rabbit), Sox2 (1µg/ml, Rabbit, Abcam ab97959), GFAP (1:500, Mouse, Sigma, G3893), β-Tubulin III (1:500, mouse, Abcam ab7751–100), Nestin (1:1000, Chicken, Abcam ab134017). After overnight incubation in primary antibodies cryosections were washed three times with PBST to remove primary antibody and incubated 1h into secondary antibodies. We used alexa fluor conjugated secondary antibodies including anti-Mouse alexa fluor 488, 594, and anti-rabbit alexa fluor 488, 594 (Molecular Probes, USA, 1µg/ml dilution in PBS). Cryosections were washed three more times with PBST to remove secondary antibody and mounted with Vectashield hardset mounting medium with nuclear stain (DAPI) following manufacturer's instructions.

qRT-PCR

For RNA extraction, 100 µL cell culture supernatant was incubated with 400 µL AVL buffer (viral lysis buffer used for purifying viral nucleic acids). For cellular RNA extraction, cells were collected in Trizol reagent and RNA was extracted by Direct-zol RNA Kit (Zymo) and quantified by qRT-PCR using gene specific primers (Table S1).

Western blotting

Human lung organoids and foregut spheroids were lysed in 200µl of RIPA buffer containing protease inhibitor cocktail (Roche) and proteins were extracted by centrifugation at 13,000×g for 10min at 4°C. Extracted proteins concentration was determined by BioRad DC protein assay kit as per manufacturer instructions (Bio-Rad) and equal amounts of protein (25µg) were resolved by SDS-PAGE and transferred to PVDF membranes. Membranes were blocked with 5% nonfat milk in PBST for 2h at room temperature followed by overnight incubation at 4°C with primary antibodies such as ECAD (1:1000, Rabbit), NKX2.1 (1:1000, Rabbit), Vimentin (1:1000, Rabbit), SOX9 (1:1000, Rabbit), FOXJ1 (1:1000, Mouse), Mucin5AC (1:1000, Rabbit), Surfactant protein B, SP-B (1:1000, Mouse), GAPDH (1:1000), ACE2 (1:1000, Rabbit) and TMPRSS2 (1:1000, Rabbit). On following day, membranes were then washed three times with tris-buffered saline with 0.1% Tween-20 (TBST) and incubated for 2h with secondary antibody conjugated with

horseradish peroxidase (HRP). Immunoreactive protein signals were detected with Supersignal West Pico Chemiluminescent Substrate (Pierce, USA).

SARS-CoV-2 pseudo virus production, titration and characterization

293FT cells were transfected with pLVX expressing SARS-CoV-2-S. Nineteen amino acids at the C terminus of SARS-CoV-2-S was deleted, given previous report that the shortened mutant has improved incorporation into the pseudovirus envelope (Fukushi et al., 2005; Hoffmann et al., 2020; Wang et al., 2020). 24h post-transfection, cells were infected with VSV pseudovirus containing Fluc or EGFP. Cells were washed four times with medium 1h post-inoculation and maintained in medium for 24h. Then supernatant containing pseudovirus was collected, centrifuged, and used or stored at -80°C.

SARS-CoV-2 pseudovirus infection and treatment with protease inhibitor and EK-1 peptide

These infections were performed according to published procedures (Wang et al., 2020). Briefly, lung organoids were pretreated with TMPRSS2 inhibitor Camostat mesylate (10 μM) for 2h and then infected with SARS-CoV-2 pseudovirus at MOI=2. After 2h infection, virus was removed and fresh medium containing Camostat mesylate was added. For EK-1 peptide, first SARS-CoV-2 pseudovirus was incubated with EK-1 peptide (10 μM) for 30min at 37^0C and then infected organoids for 2h followed by changing with fresh medium. For pseudo virus with Fluc, cells were lysed at 24h post-infection and subjected for luciferase activity assay according to manufacturer's instruction. For pseudovirus with EGFP, infection was evaluated by taking bright field and fluorescent images of LORG at 24h post-infection.

SARS-CoV-2 isolate USA-WA1/2020 infection

SARS-CoV-2 isolate USA-WA1/2020 was obtained from BEI Resources. SARS-CoV-2 was propagated and infectious units quantified by plaque assay using Vero E6 cells. Human iPSC derived lung organoids, NPCs, neurons and astrocytes were infected with SARS-CoV-2 at MOI=2 for 2h at 37°C. Then cells were washed, and fresh medium was added. At 2h, 48 and 72h post infection supernatant and infected organoids were collected and lysed using TRIzol and RNA was extracted using a Direct-zol RNA Kit (Zymo) and quantified by RT-qPCR using SARS-CoV-2 N primers.

Quantification and Statistical Analysis:

Number of independent biological replicates includes 3 for most experiments unless otherwise indicated. p-values were calculated by unpaired two-tailed Student's t test. *p < 0.05, **p < 0.01 and ***p < 0.001.

Supplemental References

Fukushi, S., Mizutani, T., Saijo, M., Matsuyama, S., Miyajima, N., Taguchi, F., Itamura, S., Kurane, I., and Morikawa, S. (2005). Vesicular stomatitis virus pseudotyped with severe acute respiratory syndrome coronavirus spike protein. J Gen Virol *86*, 2269-2274.

Hoffmann, M., Kleine-Weber, H., and Pohlmann, S. (2020). A Multibasic Cleavage Site in the Spike Protein of SARS-CoV-2 Is Essential for Infection of Human Lung Cells. Mol Cell *78*, 779-784 e775.

Leibel, S.L., Winquist, A., Tseu, I., Wang, J., Luo, D., Shojaie, S., Nathan, N., Snyder, E., and Post, M. (2019). Reversal of Surfactant Protein B Deficiency in Patient Specific Human Induced Pluripotent Stem Cell Derived Lung Organoids by Gene Therapy. Sci Rep *9*, 13450.

Miller, A.J., Dye, B.R., Ferrer-Torres, D., Hill, D.R., Overeem, A.W., Shea, L.D., and Spence, J.R. (2019). Generation of lung organoids from human pluripotent stem cells in vitro. Nat Protoc *14*, 518-540.

Wang, S., Li, W., Hui, H., Tiwari, S.K., Zhang, Q., Croker, B.A., Rawlings, S., Smith, D., Carlin, A.F., and Rana, T.M. (2020). Cholesterol 25-Hydroxylase inhibits SARS-CoV-2 and coronaviruses by depleting membrane cholesterol. EMBO J, e2020106057.